D-A--A Motif Quinoxaline-Based Sensitizers with High Molar Extinction Coefficient for Quasi-Solid-State Dye-Sensitized Solar Cells

D-A-π-A Motif Quinoxaline-Based Sensitizers with High Molar Extinction Coefficient for Quasi-Solid State Dye-sensitized Solar Cells

Yu Wang[a]†, Zhiwei Zheng[a]†, Tianyue Li[b], Neil Robertson[b], Huaide Xiang[a], Wenjun Wu[a, b]*, Jianli Hua[a], Wei-Hong Zhu[a], and He Tian[a]

[a]*Key Laboratory for Advanced Materials and Institute of Fine Chemicals, Shanghai Key Laboratory of Functional Materials Chemistry, School of Chemistry and Molecular Engineering, East China University of Science and Technology, 130 Meilong Road, Shanghai, 200237, China.*

[b]*EaStCHEM School of Chemistry, University of Edinburgh, Kings Buildings, Edinburgh EH9 3FJ, UK.*

ABSTRACT: To meet the requirement of high molar extinction coefficient, broaden absorption spectrum and photo/thermal stable for sensitizers of quasi-solid dye-sensitized solar cells (Qs-DSSCs) with reduced film thickness, a novel D-A-π-A configuration organic sensitizer **IQ22** was specifically designed, in which the conjugation bridge of cyclopentadithiophene (CPDT) unit was incorporated to widen the light response and enhance molar coefficients for increasing the short-circuit current density (J_{SC}), and the octane chain on CPDT was targeted for suppressing the charge recombination and improving the open-circuit voltage (V_{OC}). As a result, the Qs-DSSC based on

IQ22 exhibits very promising conversion efficiency as high as 8.76%, with a J_{SC} of 18.19 mA cm^{-2}, a V_{OC} of 715 mV, and a fill factor (FF) of 0.67 under AM 1.5 illumination (100 mW cm^{-2}), standing out in the Qs-DSSCs utilizing metal-free organic sensitizers.

Keywords： quinoxaline, auxiliary acceptors, sensitizer, quasi-solid state, dye-sensitized solar cells

INTRODUCTION

In the fields of dye-sensitized, perovskite and other emerging solar cell technologies, [1-6] stability issue on cell devices is recognized as an urgent problem for a new generation of practical photovoltaic devices. Although perovskite solar cells can show efficiency of more than 20%, the superiority in environmental friendliness and stability of DSSCs can be more attractive for some applications.[6] Accordingly, for low-cost, high-efficiency dye-sensitized solar cells (DSSCs), the development of acceptably stable quasi-solid-state or solid-state devices, without any volatile electrolyte solution, is critical at present. Due to facile diffusion in porous TiO_2 and the large area contact with counter electrode, the quasi-solid state dye-sensitized solar cell (Qs-DSSC) is not only conducive to a high power conversion efficiency (PCE), [7-8] but also can significantly improve the device stability, thereby becoming a hot topic in the DSSCs field. Moreover, polymer gel electrolytes have led to efficient quasi-solid electrolytes for Qs-DSSCs. [9-10]

Currently, the main practical limitations for the evolution of Qs-DSSCs are lower power conversion efficiency (PCE) arising from low electrolyte ion diffusion rates and the resulting serious electronic recombination. [11-15] In this regard, Qs-DSSCs always need thin TiO_2 electrode, and accordingly an ideal sensitizer should exhibit strong light-harvesting capability. Indeed, the desirable sensitizer with high molar extinction coefficient and broaden light response region is very critical to the thinner TiO_2 electrode-based Qs-DSSCs, in which the electronic recombination

can be distinctly repressed, and the intramolecular charge transfer (ICT) can be optimized. [16-20] Recently, a new generation of D-A-π-A motif organic sensitizers came into existence with an auxiliary acceptor group introduced into the π-bridge of the D-π-A framework, leading to excellent photovoltaic performances. [21-26] As an exemplary D-A-π-A featured dye with quinoxaline as additional unit, **IQ4** showed high PCE of 9.24% with volatile iodine electrolyte. [27] Herein we focused on how to increase molar extinction coefficients and broaden light-responsive region, thereby specifically developing targeted sensitizers for constructing high performance Qs-DSSCs.

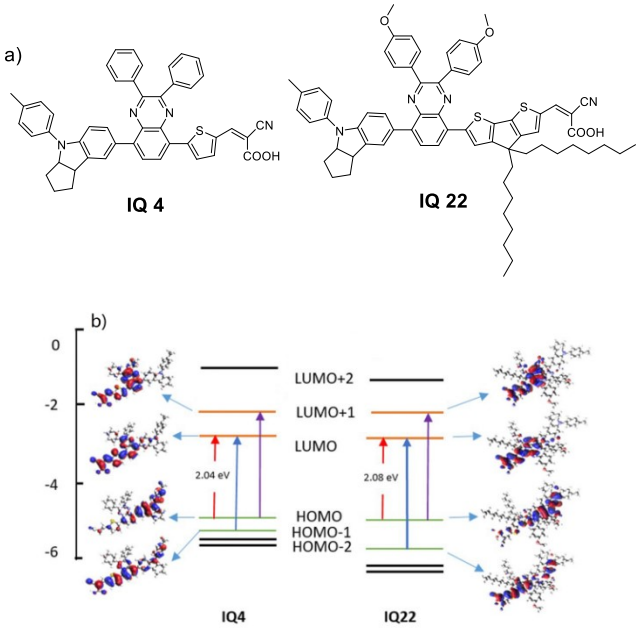

Scheme 1. a) The molecular structures of **IQ22** and **IQ4** and b) their calculated energy-level diagram and major electron-transfer absorption processes.

Based on **IQ4**, we report a new D-A-π-A DSSC sensitizer **IQ22** (shown in Scheme 1), in which the conjugation bridge of cyclopentadithiophene (CPDT) unit was incorporated to widen the light response and enhance molar coefficients for increasing the short-circuit current density (J_{SC}), the octane chain on CPDT was targeted for suppressing the reverse current and improving the open-circuit voltage (V_{OC}). As demonstrated, a commercial I^-/I_3^- polymer gel electrolyte OPV-

MPV-I was successfully exploited for fabricating Qs-DSSCs utilizing **IQ22** and **IQ4** as sensitizers, achieving high conversion efficiencies of 8.76% and 8.30% under 100 mW cm^{-2} illumination, respectively, which is an exhilarating PCE for Qs-DSSCs based on metal-free organic sensitizers. Furthermore, these devices showed excellent stability, almost maintaining the initial conversion efficiency even after 1000 h.

RESULTS AND DISCUSSION

Charge Transport Difference between Gel and Volatile Electrolytes. In order to quantify any bottleneck limiting the efficiency for Qs-DSSCs, we first performed conductivity (σ) measurements of gel and volatile electrolytes (See experimental section) with electrochemical impedance spectroscopy. [28] This offers key information about the mobility of the ions, their interaction with the solvent and any ion-pairing phenomena. As shown in Figure 1a, all plots of ln σ against 1000/T give straight lines, which is typical ion-conducting behavior follow an Arrhenius relationship. [29] In Figure 1a, the obvious difference between the gel and volatile electrolyte is the variation of the slope with measurement temperature. With increasing temperature, the conductivity of the gel electrolyte rises rapidly owing to the viscosity reduction, whereas the change for the volatile electrolyte shows a more gradual process. At room temperature, the conductivity of the gel and volatile electrolyte are 2.10×10^{-3} S cm^{-1} and 3.0×10^{-3} S cm^{-1}, respectively. In addition, Tafel polarization measurements were implemented using dummy cells with each of the different electrolytes between two Pt electrodes (Figure 1b). [30-31] In the Tafel and diffusion zone, the exchange current density (J_0) and limiting diffusion current density (J_{lim}) values lie in the order of volatile > gel for **IQ22** and **IQ4**, respectively, indicating that the gel electrolyte has some limitations in the charge-transfer and diffusion likely due to the greater viscosity. [32] As

shown in Table 1 however, the change of electrolyte did not cause a significant impact on the short-circuit current density (J_{SC}) for **IQ22** or **IQ4**.

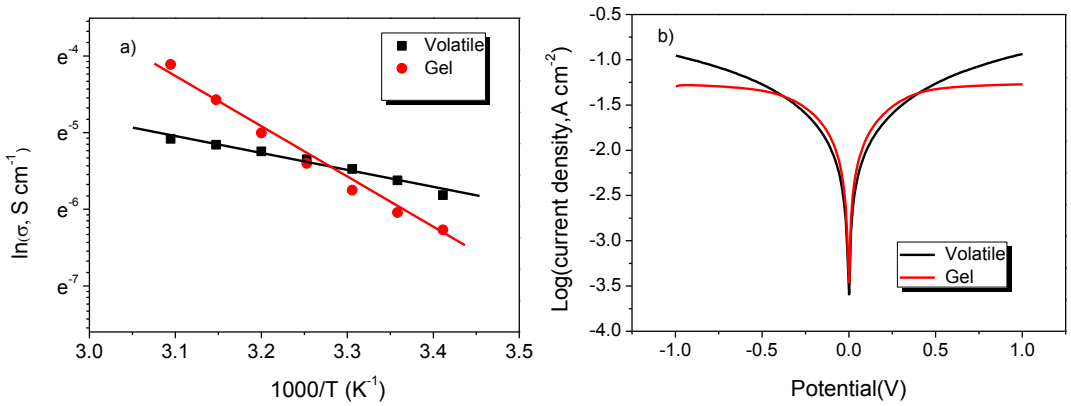

Figure 1. Temperature dependence of ionic conductivity (a) and Tafel polarization curves of symmetric dummy cells with two platinum electrodes at room temperature (b) for volatile and gel electrolytes.

Enhancement in Molar Extinction Coefficients and Light-Harvesting Capability. In DSSCs, the sensitizers with high extinction coefficients allow reduced thickness of TiO_2 electrode, which results in increase of the average optical power density within the film and decrease of the charge recombination sites, as the film becomes thicker the charges have more chance of recombining before influencing the potential at the electrodes. [33] Recently, a D-A-π-A prototype has become attractive, especially for constructing high extinction coefficients, broaden light response, and photo/thermal stable organic sensitizing dyes. [34-35] As shown in Scheme 1, for the design of sensitizer **IQ22**, we employed indoline as the electron donor since it manifested superior electron-donating capacity and led to excellent photovoltaic performance in a number of efficient D-A-π-A sensitizers. [36-38] We also used the standard group cyanoacetic acid as the acceptor/anchor unit. For an ideal sensitizer, high molecular extinction coefficient and broad wavelength response are highly preferable for high-efficiency DSSCs. On the basis of the rational molecular design, the

structure modification in this report was conducted by introducing the high conjugation building block of CPDT as π bridge (**IQ22**), instead of the thiophene unit (**IQ4**). In particular, dye **IQ22** exhibits appropriate photo-physical properties, such as a higher molecular extinction coefficient and broad light response region. The addition of two methoxy groups in the auxiliary (quinoxaline) unit can fine-tune and optimize the E_{OX} (The first oxidation potential) and E^*_{RED} (The excited-state reduction potential), through certain electron-donating character. In addition, octyl groups were grafted onto the CPDT unit to reduce aggregation and to address the serious electronic recombination in Qs-DSSCs. [11-15] The synthetic route is presented in Figure S1.

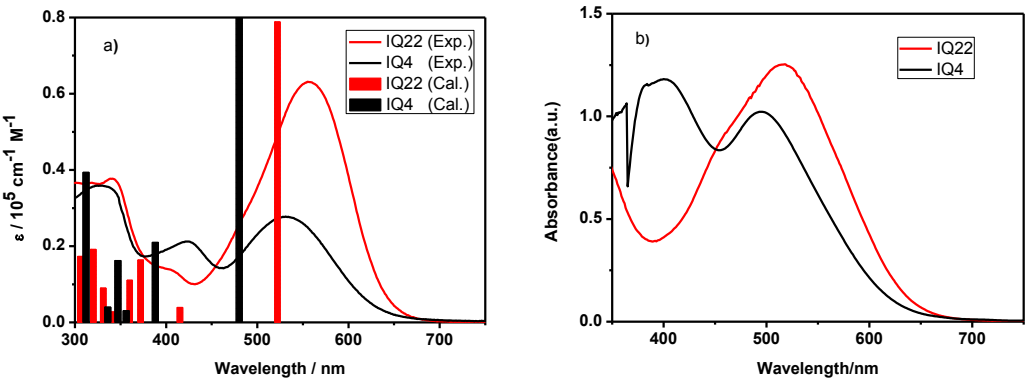

Figure 2. Absorption spectra of **IQ22** and the reference dye **IQ4**. a) The experimental spectra (in CH_2Cl_2) are shown as continuous lines and the theoretical electronic transitions are shown as bars for both **IQ22** (red) and **IQ4** (black). Theoretical data were computed using TD-DFT (CH_2Cl_2) and b) The experimental spectra on 4 μm TiO_2 thin film.

Experimental and Calculated Absorption Properties. To preliminarily estimate the effect of structure modification on the light-harvesting capacity for **IQ22**, we tested the UV-Vis absorption spectra of the two dyes in CH_2Cl_2 (Figure 2a) and their corresponding data are summarized in Table 1. Both dyes show two distinct absorption bands at about 325 and 540 nm, corresponding to the π-π* and ICT bands, respectively. With respect to **IQ4**, **IQ22** presents a notable bathochromic

shift in the maximum visible absorption wavelength from 531 to 555 nm, which arises from the introduction of a large π-linker CPDT unit. As expected, replacing the thiophene unit (in **IQ4**) with CPDT (in **IQ22**) is beneficial for greatly enhancing the molar extinction coefficient (up to 63200 M^{-1} cm^{-1}, 2.47-fold greater than that of the reference dye **IQ4**) and light-harvesting with red shift in absorption band, which are the preconditions for obtaining a high photocurrent output. Upon loading on TiO_2 films (Figure 2b), both dyes show hypsochromic shift from 531 to 497 nm for **IQ4** and from 555 to 516 nm for **IQ22**, due to the deprotonation of the cyanoacetic acid group. Obviously, **IQ22** shows a higher and broader spectrum in the visible region relative to **IQ4**. On the other hand, the broader peak width on the films indicate that aggregation inevitably occurs to some extent in these films for both dyes. The high molar extinction coefficient and wide absorption spectrum for **IQ22** exactly cater to the reduced film thickness requirements of Qs-DSSCs since the charge recombination and diffusion problems in nano-porous membrane.

Electronic structures of **IQ4** and **IQ22** were calculated and investigated with DFT calculations. The selected Kohn-Sham (KS) molecular orbital distributions and energies of **IQ4** and **IQ22** are shown in Table S1 and Table S2, respectively. For both **IQ4** and **IQ22**, the KS HOMO is mainly located on the strong electron-donating unit of indoline, while more centralized on indoline group for **IQ22**. The location of KS LUMO is on the electron-withdrawing unit of cyanoacetic acid, and was not affected by the alkane chains added. In Scheme 1, the energy level schemes of selected Kohn-Sham orbitals of **IQ4** and **IQ22** are shown, indicating good charge separation after excitation by photons.

Time-dependent DFT (TDDFT) calculations allow comparison of absorption spectroscopy both experimentally and theoretically, and thus the electronic transitions were studied (Figure 2a). The TDDFT calculations for **IQ4** and **IQ22** show broadly good agreement with experimental

absorption spectra, and the pathways for excitation and electron injection process can be learned by studying the computational results. For **IQ22**, the first electronic transition, which is calculated to be at 521 nm, is characterized by HOMO → LUMO contribution (52%) and HOMO-1 → LUMO contribution (39%), and the absorption at 413 nm is mainly composed of HOMO → LUMO +1 (47%) and HOMO-1 → LUMO (29%). For **IQ4**, the calculated low-energy electronic transition (at 483 nm) is composed of HOMO → LUMO (69%) and HOMO -1 → LUMO (21%), and the second electronic transition (at 384 nm) is composed of HOMO -1 → LUMO (51%) and HOMO → LUMO +1 (23%). The lowest energy transition for both dyes is dominated by exciting electrons from HOMO to LUMO orbitals, and the oscillator strength is nearly doubled through structural modification for **IQ22**.

Experimental Energy Levels and Orbital Distributions. The electrochemical characterization combined with UV-Vis spectrum can be used to estimate the molecular energy level position and distribution. As shown in Figure S2 (cyclic voltammetry curves), the first redox potentials (E_{OX}) for **IQ22** and **IQ4** are 0.82 and 0.61 V (vs NHE) (shown in Table 1), respectively. The introduction of methoxy units into **IQ22** shifts E_{OX} 0.21 V negative due to its electronic donor property. Correspondingly, estimated from the optical gap $E_{0\text{-}0}$ (from the absorption thresholds of the UV-Vis spectra) and E_{OX}, the excited state reduction potentials (E^*_{RED}) of dyes **IQ22** and **IQ4** are -1.10 and -1.32 V, respectively. Due to an almost unchanged $E_{0\text{-}0}$, dye **IQ22** shows a lower E^*_{RED} value due to its E_{OX} level lying at lower energy compared with **IQ4**. The orbital distributions and the E_{OX} and E^*_{RED} values are expected to ensure strong directionally efficient electron injection into the conduction band of TiO_2. This did not influence the current of Qs-DSSCs based on **IQ22** thanks to it located in essential energy level scope.[38] Moreover, the other difference of CV curves for **IQ22** and **IQ4** is two pairs of submits were

observed for **IQ22**. In previous investigations, for the sensitizer based on quinoxaline group with alkoxy chains [39], a single oxidation peak appeared in its CV curve, but for that containing CPDT unit [40, 41], two obvious oxidation peaks were got. Therefore, two oxidation peaks in CV for **IQ22** is owing to CPDT unit was involved in the redox process in addition to the electron donor indoline.

Solar Cell Performances. To compare the photovoltaic performance of Qs-DSSCs with the traditional volatile-electrolyte iodine-based devices, we prepared a set of devices sensitizing 8 μm

Table 1. Photophysical and electrochemical properties of sensitizers and photovoltaic parameters of DSSCs based on **IQ22** and **IQ4** with volatile and gel electrolyte.

Dyes[a]	λ_{max}[b]	ε[b]	λ_{max}[c]	E_{OX}[d]	$E_{0\text{-}0}$[e]	E^*_{RED}[f]	J_{SC}	V_{OC}	*FF*	η[g]
	nm	M^{-1} cm^{-1}	nm	V	eV	V	mA cm^{-2}	mV		
IQ22-V	555	63200	516	0.82	1.92	-1.10	18.36	748	0.72	9.83
IQ22-G							18.19	715	0.67	8.76
IQ4-V	531	25700	497	0.61	1.93	-1.32	17.58	743	0.73	9.51
IQ4-G							17.44	707	0.67	8.30

Note: [a] V: Volatile electrolyte; G: Gel electrolyte. [b]Absorption parameters were obtained in CH_2Cl_2. [c]Absorption parameters were obtained on 4 μm nanocrystalline TiO_2 film. [d]The E_{OX} was obtained in CH_2Cl_2 with ferrocene (0.63 V vs. NHE) as external reference. [e]$E_{0\text{-}0}$ values were estimated from the wavelength at 10% maximum absorption intensity for the dye-loaded 3 μm nanocrystalline TiO_2 film. [f]The E^*_{RED} was calculated according to $E^*_{RED} = E_{OX} - E_{0\text{-}0}$.

(4 μm transparent layer + 4 μm scattering layer) mesoporous TiO_2 films with sensitizer **IQ22** or **IQ4**. The current-voltage (*J-V*) curves of devices measured under Am 1.5G illumination (100 mW cm^{-2} at 298 K) are shown in Figure 3, with the corresponding photovoltaic parameters listed in Table 1. As a result, using volatile iodine electrolyte, we obtained a solar-to-electric conversion efficiency of 9.83 % (J_{SC} = 18.36 mA cm^{-2}, V_{OC} = 748 mV, *FF* = 0.72) and 9.51% (J_{SC} = 17.58 mA cm^{-2}, V_{OC} = 743 mV, *FF* = 0.73) based on **IQ22** and **IQ4**, respectively. In contrast, the PCEs are 8.76 % (J_{SC} = 18.19 mA cm^{-2}, V_{OC} = 715 mV, FF = 0.67) and 8.30 % (J_{SC} = 17.44 mA cm^{-2},

V_{OC} = 707 mV, FF = 0.68) for **IQ22** and **IQ4** with gel electrolyte, respectively. Due to poorer charge transport in viscous quasi-solid electrolyte, the electronic recombination probability increases, resulting in the open-circuit voltage reduction for **IQ22-**G and **IQ4-**G compared with **IQ22-**V and **IQ4-**V, respectively. Of great significant, no matter with volatile or gel electrolyte, we obtained almost the same photocurrent, which is of great importance to the development of stable DSSCs with high power conversion in the future. It also indicates the preferable electron injection and regeneration performance for the IQs sensitizer, especially for **IQ22**. Notably, J_{SC} estimated from IPCE spectra are broadly comparable with those obtained from the *J–V* curves, and the integration of IPCE curve for **IQ22-**V, **IQ22-**G**, IQ4-**V and **IQ4-**G are 17.69, 17.33, 16.85 and 16.69 mA cm^{-2}, respectively. The slightly lower values may be interpreted in terms of more efficient charge transport and collection[42] due to a thermal effect associated with the full sunlight irradiation.[43]

The Impact of Molecular Structure on Short-Circuit Photocurrent. With the same assembling condition for devices, the contribution to the enhancement of photocurrent can be attributed to the improvement of the sensitzer's photoresponse region, absorption intensity and energy levels.

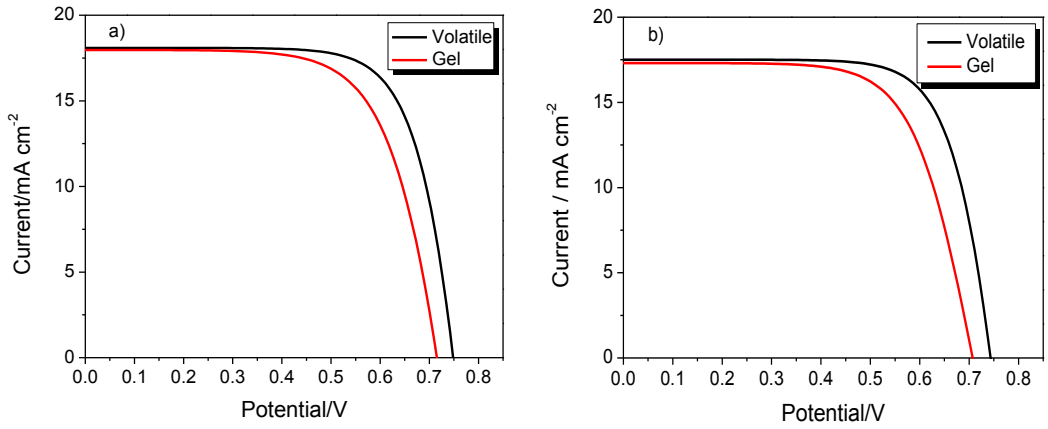

Figure 3. The *J*-V curves for DSSCs based on **IQ22** (a) and **IQ4** (b) with volatile and gel electrolyte.

As shown in Figure 4a, the light harvesting efficiency (LHE) spectra were calculated from the absorption spectra of the dye-loaded TiO_2 films (LHE = $1\text{-}10^{-\alpha}$, where α is the intensity of the light absorption). [44] For **IQ22**, the expanded conjugated system with CPDT improves the molar extinction coefficient and broadens the absorption spectrum, so its LHE showed significant enhancement in the visible range of 450-700 nm. To shed light on the contribution of absorption at different wavelengths to the J_{SC}, we also measured the incident-photon-to-current conversion efficiency (IPCE) action spectra for the DSSCs based on the **IQ22** and **IQ4** with volatile or gel electrolyte (Figure 4b). As shown in Figure 4b, almost all the IPCE values between 300-800 nm slightly decrease for the gel electrolyte with **IQ22** or **IQ4**, which is due to its higher viscosity hence lower conductivity. But for **IQ22** compared with **IQ4**, the higher and broader IPCE spectrum with volatile or gel electrolyte can be attributed to its larger conjugated system and branched structure further improving the intramolecular charge separation and charge recombination inhibitory ability which is highly beneficial to the J_{SC} of Qs-DSSC.

The Determinants of Open-Circuit Voltage. Electrochemical impedance spectroscopy was used to investigate the origin of the V_{OC} variation for DSSCs sensitized with **IQ22** and **IQ4**. According to reference, [45] there are two main factors that result in the variation of DSSC V_{OC}. The first is a conduction band shift and the second is recombination of injected electrons with the oxidized sensitizer or electrolyte.

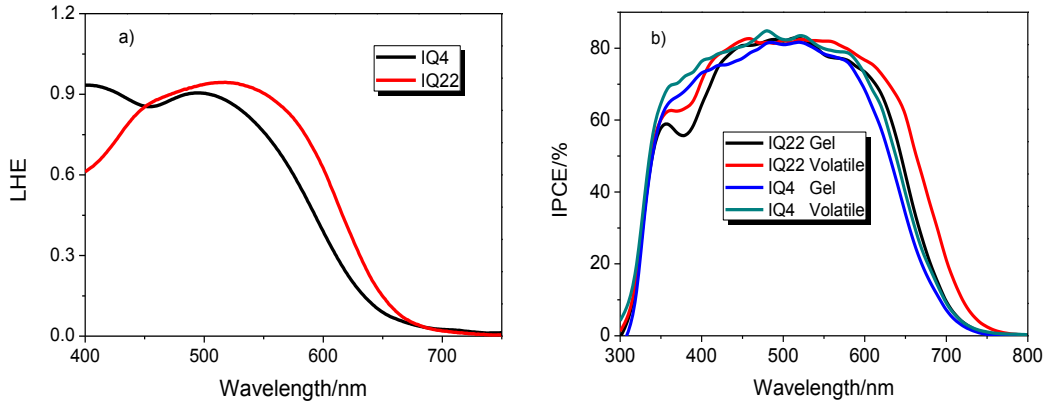

Figure 4. a) LHE spectra calculated from the absorption spectra of dye-loaded TiO_2 film; b) IPCE spectra of DSSCs sensitized by **IQ22** and **IQ4** with gel or volatile electrolyte.

As a downward shift of the TiO_2 conduction band would increase the density of occupied states (DOS) which are directly proportional to chemical capacitance (C_{chem}), [45] measurement of C_{chem} as a function of potential bias allows insight into the DOS in devices made with different dyes. As presented in Figure 5a and b, C_{chem} is lower for **IQ22** with both electrolytes at a given voltage indicating an upward shift of the conduction band due to the increase of dipole. [46] It indicates the upward shift of the conduction band as one of the origins for the increase V_{OC} in **IQ22**-sensitized DSSCs (as listed in Table 1).

To obtain insight into the electron recombination occurring between excited electrons in the conduction band and sensitizers or electrolyte, the electron lifetimes were explored as a function of potential bias (Figure 5c and d). At a given potential, the electron lifetime in cell sensitized with **IQ22** was obviously longer than that with **IQ4** based on gel (Figure 5c) or volatile electrolyte (Figure 5d). It further demonstrates that the branched alkyl chains for **IQ22** effectively suppress the electron recombination on the TiO_2 surface improving the electron lifetime. Especially, the major difference in lifetime for gel electrolytes (Figure 5c) with the serious charge recombination

reflects the superior suppressing effect of the branched structure in **IQ22**. Therefore, the longer electron lifetime is another origins for the higher V_{OC} of **IQ22**.

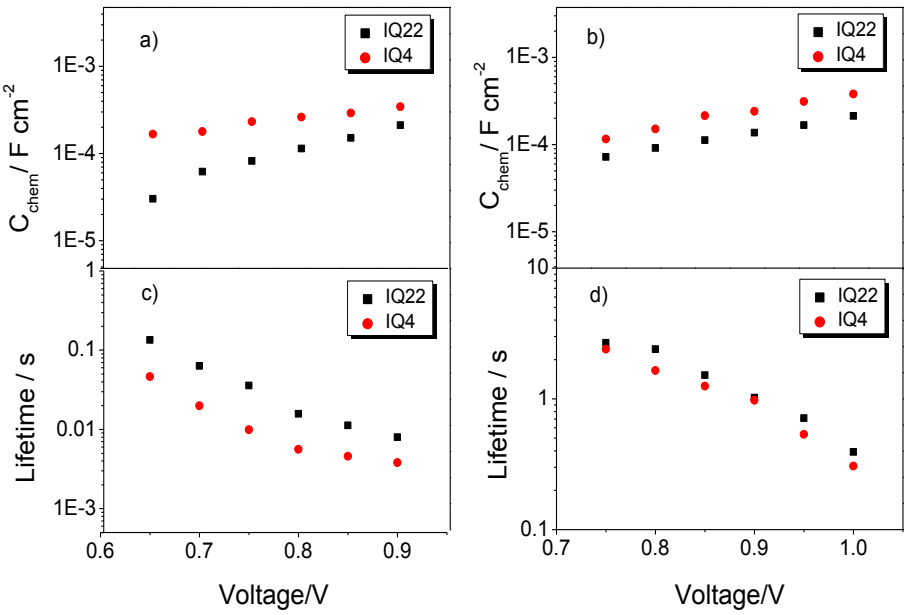

Figure 5. Chemical capacitance and electron lifetime as a function of bias potential obtained through electrochemical impedance spectroscopy carried out on devices with gel electrolyte (a, c) and volatile electrolyte (b, d), respectively in the dark.

The Stability of Photovoltaic Performance. To develop Qs-DSSCs, we mainly aimed at the improvement of their thermal and light-exposure stability. As presented in Figure 6, the photovoltaic performance of Qs-DSSCs exhibited excellent stability during a 1000 h accelerated aging for **IQ22** and **IQ4**-based cells with gel electrolyte in a solar simulator under full intensity (100 mW cm $^{-2}$) at 50 °C. [47] In the long term light and thermal environment, the enhancement of J_{SC} from 0 to 100h especially for **IQ4** indicated the system changes gradually stabilized due to the improvement of the interfacial contact between TiO_2 and electrolyte. [48] The J_{SC} increased significantly at this stage, resulting in an increase in efficiency, although V_{OC} and *FF* changed slightly to lower values. Along with the increase in J_{SC}, V_{OC} decreased because more electron recombination can occur with passage of time. In the light-soaking from 100 to 1000 h, however,

all four photovoltaic parameters remained almost constant, which shows not only the good stability of quasi-solid electrolyte, but also the excellent anti-decomposition property exposure to light and heat for IQs dyes.

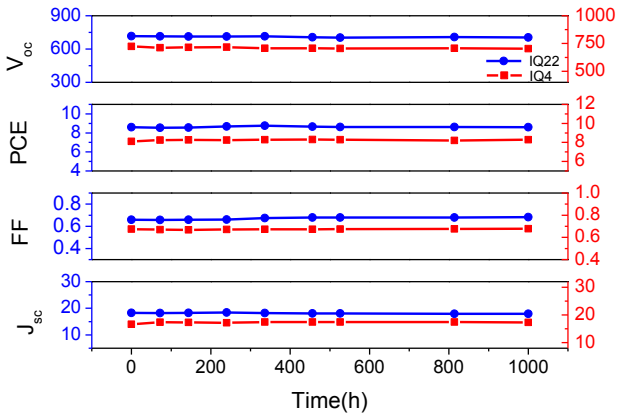

Figure 6. Stability test of photovoltaic parameters (V_{OC}, PCE, *FF* and J_{SC}) variation with aging time for the devices based on **IQ22** (blue line) and **IQ4** (red line) with quasi-solid-state electrolyte during 1 sun visible-light soaking at 50 °C.

CONCLUSIONS

In summary, we have demonstrated **IQ22** as an effective sensitizer for Qs-DSSC devices, with a high power conversion efficiency. For the optimum Qs-DSSC based on **IQ22**, a metal-free organic sensitizer, the PCE reached 8.76 % with high J_{SC} (18.19 mA cm^{-2}). Due to the lower conductivity and higher charge recombination for the gel electrolyte, the superior performance can be attributed to the structural design with high conjugation unit (broadening the photoresponse spectrum) and branched alkyl chains (boosting the electronic recombination suppression). As a consequence, no matter which electrolyte we choose, the determining factors for the higher open-circuit voltage of **IQ22** compared with **IQ4** are its positive shift of conduction band and longer electronic lifetime. Overall, we obtain efficient and stable DSSCs, using low-cost organic sensitizers for Qs-DSSCs with excellent energy matching properties, advancing the practical application of DSSCs.

EXPERIMENTAL SECTION

Cell Assembly: The working electrode was composed of an 8 μm thick TiO_2 film, including a 4 μm transparent layer with 18 NRT and 4 μm scattering layer with 18NR-AO. The dye solutions were 0.3 mM in chloroform/ethanol (3/7) and the photoanodes underwent dipping for 12 h to complete the loading with sensitizers. The dye-covered TiO_2 electrode and Pt-counter electrode were assembled into a sandwich type cell and sealed with a hot-melt gasket of 45 μm thickness made of the ionomer Surlyn 1702 (DuPont) with a heat sealing machine. The size of TiO_2 electrodes used was 0.25 cm^2 (i.e., 5 mm×5 mm). For the liquid state device, a drop of the electrolyte was put on the hole in the back of the counter electrode. It was introduced into the cell via vacuum backfilling. The hole in the counter electrode was sealed by an aluminum foil tape. For the Qs-DSSCs, the electrolyte was spreaded on the TiO_2 film before packaging with Surlyn ring and Pt electrode and then hot-pressed. Both conductivity and Tafel polarization curves were recorded by assembling symmetric dummy cells consisting of Pt CE|electrolyte|Pt CE. The volatile iodine electrolyte contained: 0.5 M BMII (1-butyl-3-methylimidazolium iodide), 0.1 M DMPII (1, 2-dimethyl-3-propylimidazolium iodide), 0.05 M I_2, 0.1 M LiI, 0.1 M GuSCN (guanidinium thiocyanate) and 0.5 M 4-tert-butylpyridine in a mixture of acetonitrile and valeronitrile (volume ratio, 85 : 15). The polymer gel electrolyte (OPV-MPV-I) was a product of Yingkou OPV Tech New Energy Co, Ltd. (Liaoning, China), and it contains polymer, LiI, 3-methoxypropionitrile (MPN), I_2, guanidine thiocyanate (GuSCN) and 4-tert-butylpyridine (TBP). [9-10]

SYNTHESIS AND CHARACTERIZATION OF COMPOUNDS:

Synthesis of IQ22a. The unpurified indoline borate THF solution was reacted with 5,8-dibromo-2,3-(4-methoxyphenyl) quinoxaline (1.0 g, 2.72 mmol) under Suzuki coupling reaction using $Pd(PPh_3)_4$ (40 mg) and K_2CO_3 aqueous solution (30 mL, 2 M) as catalysts in 80 mL THF for 12

h. After cooling, water was added and the reaction mixture was extracted with CH_2Cl_2. The combined organic layer was washed with H_2O and brine, dried over anhydrous Na_2SO_4, and evaporated under reduced pressure. The crude product was purified by column chromatography (CH_2Cl_2/PE = 1/3) on silica gel and the product was obtained as a red solid, 22a (270 mg, 0.61 mmol, 72%).1H NMR (400 MHz, DMSO-d_6, δ): 7.88 (d, J = 8 Hz, 1H), 7.82 (d, J = 8 Hz, 1H), 7.56-7.70 (m, 5H), 7.13 (d, J = 4.8 Hz, 1H), 6.84-6.92 (m, 3H), 6.82 (d, J = 8.0 Hz, 2H), 3.79 (s, 3H), 3.77 (s, 3H), 1.75-1.89 (m, 4H), 1.02-1.15 (m, 20H), 0.88-1.00 (m, 4H), 0.74 (t, J=5.8 Hz, 6H). 13C NMR (100 MHz, DMSO-d_6, δ):159.62, 159.49, 157.50, 156.63, 151.52, 150.68, 140.12, 137.52, 136.98, 136.37, 135.91, 132.24, 131.54, 130.88, 130.63, 130.04, 129.88, 124.83, 124.32, 120.64, 120.32, 120.00, 112.79, 54.29, 52.42, 36.88, 30.78, 29.10, 28.34, 28.27, 23.61, 21.59, 13.05.

Synthesis of IQ22b. 5 mL of dry dimethylformamide (DMF) was dissolved in 10 mL CH_2Cl_2 and cooled in an ice bath to 0ºC. In a separate vessel, 3 mL of phosphorus oxychloride was dissolved in 5 mL CH_2Cl_2, and this solution was added to the solution of DMF dropwise with continuous stirring at 0 ºC for 1 hour. After the addition was complete, 22a dissolved in 20 mL of CH_2Cl_2 was added, dropwise with stirring. The solution was brought to room temperature overnight. The mixture was washed with water and extracted with CH_2Cl_2 until the color was removed. The combined organic extract was dried over sodium sulfate, Na_2SO_4, and evaporated to remove solvent under reduced pressure. The origin oil obtained was purified by column chromatography (CH_2Cl_2/PE = 2/3) and the product was obtained as an orange solid, 22b (220mg , 68%).1H NMR (400 MHz, $CDCl_3$, δ): 9.84 (s, 1H, -COH), 7.99 (d, J=8.1 Hz, 1H, Ph-H), 7.91 (m, J=8.1 Hz, 1H, Ph-H), 7.74 (s, 1H, thienyl-H), 7.66~7.72 (m, 4H, Ph-H), 7.65 (s, 1H, thienyl-H), 6.87~6.98 (m, 4H, Ph-H), 3.89 (s, 3H, -O-CH_3), 3.86 (s, 3H, -O-CH_3), 1.56 (s, 6H, -C-CH_3).

Synthesis of 22c. The indoline borate THF solution was prepared from 7-bromo-1,2,3,3a,4,8b-hexahydro-4-(4-methylphenyl)-cyclopent[b]indole (160 g, 0.50 mmol). The unpurified indoline borate THF solution was reacted with 22b (200 mg, 0.25 mmol) under Suzuki coupling reaction using $Pd(PPh_3)_4$ (10 mg, 8 mmol) and K_2CO_3 aqueous solution (4 mL, 2 m) as catalysts in 15 mL THF for 12 h. After cooling, water was added and the reaction mixture was extracted with CH_2Cl_2. The combined organic layer was washed with H_2O and brine, dried over anhydrous Na_2SO_4, and evaporated under reduced pressure. The crude product was purified by column chromatography (CH_2Cl_2/PE = 1/2) on silica gel and the product as obtained as a deep red solid, 21c (150 mg, 0.16 mmol, 64%). 1H NMR (400 MHz, $CDCl_3$, δ): 9.93 (s, 1H), 8.21 (d, J=8 Hz ,1H), 7.85-7.87 (m, 4H), 7.82 (s, 1H), 7.73 (d, J=8.8 Hz, 2H), 7.67 (s, 1H), 7.61-7.63 (m, 1H), 7.31 (d, J=8.4 Hz, 2H), 7.24 (d, J=8 Hz,2H), 7.13 (d, J=8.4 Hz, 1H), 7.05 (d, J=8.8 Hz, 2H), 6.91 (d, J=8.8 Hz, 2H), 4.88-4.95 (m, 1H), 3.96-3.98 (m, 4H), 3.87 (s, 3H), 2.47-2.58 (m, 3H) , 2.10-2.25 (m, 2H) , 1.98-2.08 (m, 5H) , 1.86-1.95 (m, 1H) , 1.72-1.82 (m, 2H) , 1.20-1.32 (m, 20H) , 1.10-1.19 (m, 4H) , 0.89-1.38 (m, 6H). 13C NMR (100MHz, $CDCl_3$, δ): 182.45, 161.94, 160.54, 160.34, 157.95, 150.88, 150.68, 148.78, 147.84, 144.74, 143.10, 140.43, 139.40, 138.90, 138.48, 136.97, 134.54, 131.90, 131.72, 131.61, 131.42, 131.29, 130.19, 130.08, 129.84, 128.37, 128.02, 127.81, 126.65, 120.02, 113.91, 107.26, 69.22, 55.38, 55.31, 53.91, 45.62, 37.94, 35.16, 33.88, 31.89, 30.16, 29.45, 29.37, 24.80, 24.65, 22.71, 20.89, 14.19.

Synthesis of IQ22. A mixture of aldehyde 22c (150 mg, 0.16mmol) and cyanoacetic acid (17 mg, 0.20 mmol) in acetonitrile (16mL) was refluxed in the presence of piperidine (0.5 mL) for 7 h under argon. After it cooled, the mixture was diluted with CH_2Cl_2, washed with water and brine, dried over Na_2SO_4, and evaporated under reduced pressure. The crude product was purified by column chromatography with 1% acetic acid in CH_2Cl_2 on silica gel to yield the product as a purple

powder. 1H NMR (400 MHz, THF-d_8, δ): 8.18(d, J=8 Hz, 1H), 7.87(s, 1H), 7.72(d, J=8 Hz, 1H), 7.68(d, J=4 Hz, 2H), 7.66(d, J=4Hz, 2H), 7.53(d, J=12 Hz, 2H), 7.43(d, J=12Hz, 1H), 7.16(d, J=8Hz, 2H), 7.05(d, J=8 Hz, 2H), 6.90(d, J=8 Hz, 3H), 6.76(d, J=8 Hz, 2H), 4.80(t, J=8 Hz, 1H), 3.83(t, J=8 Hz, 1H), 3.75(s, 1H), 3.68(s, 3H), 2.21(s, 3H), 1.90-1.96(m, 6H), 1.0-1.15(m, 20H),0.95-0.99(m,4H), 0.71(t, J=5.8 Hz, 6H). 13C NMR (400 MHz, THF-d_8, δ):160.28, 140.07, 136.22, 131.17, 130.86, 130.52, 129.29, 129.10, 128.25, 128.19, 127.94, 127.15, 125.86, 119.26, 112.86, 54.36, 54.26, 53.19, 45.04, 38.13, 33.18, 31.42, 31.32, 29.61, 29.14, 28.88, 25.11, 24.39, 23.76, 22.04, 13.05. HRMS (ESI, m/z, $[M + H]^+$). Calcd for $C_{69}H_{72}N_4O_4S_2$: 1085.5073. Found: 1085.5081.

Computational methods. The molecular structures of **IQ4** and **IQ22** were firstly optimised under vacuum condition, with the starting geometries entered from software Avogadro. [49] Then from the optimised geometry from vacuum, further optimization was carried out with the presence of dichloromethane polarizable continuum model (PCM). All the calculations were performed using Gaussian 09 (R. A. Gaussian 09, M. J. Frisch, G. W. Trucks, H. B. Schlegel et al. Gaussian, Inc., Wallingford CT, 2009.) with hybrid B3LYP functional level of theory and standard 6-31G (d) basis set. Time-dependent DFT calculations (TD-DFT) [50-51] were carried out using Gaussian 09 program with PCM in Dichloromethane. CAM-B3LYP functional [52] was used, and total of 70 lowest singlet electronic transitions were calculated and further processed with GaussSum software package. [53]

ASSOCIATED CONTENT

Supporting Information. Electronic Supplementary Information (ESI) available: See DOI: 10.1039/x0xx00000x including *Materials and Characterization*, *Synthesis and characterization of compounds* and *Density Functional Theory (DFT) Calculation*.

AUTHOR INFORMATION

Corresponding Author

*Fax: (+86) 21-64252288. E-mail: wjwu@ecust.edu.cn.

Author Contributions

Yu Wang[a] and Zhiwei Zheng[a] contributed equally to this work.

Notes

The authors declare no competing financial interest.

ACKNOWLEDGEMENTS

This work was supported by NSFC for Creative Research Groups (21421004), the Programme of Introducing Talents of Discipline to Universities(B16017) and Distinguished Young Scholars (21325625), NSFC/China, Oriental Scholarship, Fundamental Research Funds for the Central Universities (WJ1416005 and WJ1315025), and the Scientific Committee of Shanghai (14ZR1409700 and 15XD1501400) for financial support.

REFERENCE

(1) Mei, A.; Li, X.; Liu, L.; Ku, Z.; Liu, T.; Rong, Y.; Xu, M.; Hu, M.; Chen, J.; Yang, Y., A Hole-Conductor–Free, Fully Printable Mesoscopic Perovskite Solar Cell with High Stability. *Science* **2014**, *345* (6194), 295-298.

(2) You, J.; Yang, Y. M.; Hong, Z.; Song, T.-B.; Meng, L.; Liu, Y.; Jiang, C.; Zhou, H.; Chang, W.-H.; Li, G., Moisture Assisted Perovskite Film Growth for High Performance Solar Cells. *Appl. Phys. Lett.* **2014**, *105* (18), 183902-183905.

(3) Kakiage, K.; Aoyama, Y.; Yano, T.; Otsuka, T.; Kyomen, T.; Unno, M.; Hanaya, M., An Achievement of Over 12 Percent Efficiency in an Organic Dye-Sensitized Solar Cell. *Chem. Commun.* **2014,** *50* (48), 6379-6381.

(4) Yao, Z.; Zhang, M.; Wu, H.; Yang, L.; Li, R.; Wang, P., Donor/acceptor Indenoperylene Dye for Highly Efficient Organic Dye-Sensitized Solar Cells. *J. Am. Chem. Soc.* **2015,** *137* (11), 3799-3802.

(5) Zeng, W.; Cao, Y.; Bai, Y.; Wang, Y.; Shi, Y.; Zhang, M.; Wang, F.; Pan, C.; Wang, P., Efficient Dye-Sensitized Solar Cells with an Organic Photosensitizer Featuring Orderly Conjugated Ethylenedioxythiophene and Dithienosilole Blocks. *Chem. Mater.* **2010,** *22* (5), 1915-1925.

(6) Bi, D.; Yi, C.; Luo, J.; Décoppet, J.-D.; Zhang, F.; Zakeeruddin, Shaik M.; Li, X.; Hagfeldt, A.; Grätzel, M., Polymer-Templated Nucleation and Crystal Growth of Perovskite Films for Solar Cells with Efficiency Greater than 21%. *Nat. Energy* **2016,** DOI: 10.1038/NENERGY.2016.142.

(7) Jia, X.; Zhang, W.; Lu, X.; Wang, Z.-S.; Zhou, G., Efficient Quasi-Solid-State Dye-Sensitized Solar Cells Based on Organic Sensitizers Containing Fluorinated Quinoxaline Moiety. *J. Mater. Chem. A* **2014**, *2* (45), 19515-19525.

(8) Lan, T.; Lu, X.; Zhang, L.; Chen, Y.; Zhou, G.; Wang, Z.-S., Enhanced Performance of Quasi-Solid-State Dye-Sensitized Solar Cells by Tuning the Building Blocks in D–(π)–A′–π–A Featured Organic Dyes. *J. Mater. Chem. A* **2015**, *3* (18), 9869-9881.

(9) Wang, C.; Wang, L.; Shi, Y.; Zhang, H.; Ma, T., Printable Electrolytes for Highly Efficient Quasi-Solid-State Dye-Sensitized Solar Cells. *Electrochim. Acta* **2013**, *91*, 302-306.

(10) Zhou, Q.; Chen, S.; Zhang, M.; Wang, L.; Li, Y.; Shi, G., Solution‐Processed Graphene Composite Films as Freestanding Platinum‐Free Counter Electrodes for Bendable Dye Sensitized Solar Cells. *Chin. J. Chem.* **2016**, *34* (1), 59-66.

(11) Stergiopoulos, T.; Rozi, E.; Hahn, R.; Schmuki, P.; Falaras, P., Enhanced Open‐Circuit Photopotential in Quasi‐Solid‐State Dye‐Sensitized Solar Cells Based on Polymer Redox Electrolytes Filled with Anodic Titania Nanotubes. *Adv. Energy Mater.* **2011**, *1* (4), 569-572.

(12) Wang, M.; Pan, X.; Fang, X.; Guo, L.; Liu, W.; Zhang, C.; Huang, Y.; Hu, L.; Dai, S., A New Type of Electrolyte with a Light‐Trapping Scheme for High‐Efficiency Quasi‐Solid‐State Dye‐Sensitized Solar Cells. *Adv. Mater.* **2010**, *22* (48), 5526-5530.

(13) Liu, B.; Wu, W.; Li, X.; Li, L.; Guo, S.; Wei, X.; Zhu, W.; Liu, Q., Molecular Engineering and Theoretical Investigation of Organic Sensitizers Based on Indoline Dyes for Quasi-Solid State Dye-Sensitized Solar Cells. *Phys. Chem. Chem. Phys.* **2011**, *13* (19), 8985-8992.

(14) Wu, W.; Yang, J.; Hua, J.; Tang, J.; Zhang, L.; Long, Y.; Tian, H., Efficient and Stable Dye-Sensitized Solar Cells Based on Phenothiazine Sensitizers with Thiophene Units. *J. Mater. Chem.* **2010**, *20* (9), 1772-1779.

(15) Tang, J.; Wu, W.; Hua, J.; Li, J.; Li, X.; Tian, H., Starburst Triphenylamine-based Cyanine Dye for Efficient Quasi-Solid-State Dye-Sensitized Solar Cells. *Energy Environ. Sci.* **2009**, *2* (9), 982-990.

(16) Qin, H.; Wenger, S.; Xu, M.; Gao, F.; Jing, X.; Wang, P.; Zakeeruddin, S. M.; Grätzel, M., An Organic Sensitizer with a Fused Dithienothiophene Unit for Efficient and Stable Dye-Sensitized Solar Cells. *J. Am. Chem. Soc.* **2008**, *130* (29), 9202-9203.

(17) Hwang, S.; Lee, J. H.; Park, C.; Lee, H.; Kim, C.; Park, C.; Lee, M.-H.; Lee, W.; Park, J.; Kim, K., A Highly Efficient Organic Sensitizer for Dye-Sensitized Solar Cells. *Chem. Commun.* **2007**, (46), 4887-4889.

(18) Wang, M.; Xu, M.; Shi, D.; Li, R.; Gao, F.; Zhang, G.; Yi, Z.; Humphry‐Baker, R.; Wang, P.; Zakeeruddin, S. M., High‐Performance Liquid and Solid Dye‐Sensitized Solar Cells Based on a Novel Metal‐Free Organic Sensitizer. *Adv. Mater.* **2008**, *20* (23), 4460-4463.

(19) Yao, Z.; Zhang, M.; Wu, H.; Yang, L.; Li, R.; Wang, P., Donor/acceptor Indenoperylene Dye for Highly Efficient Organic Dye-Sensitized Solar Cells. *J. Am. Chem. Soc.* **2015**, *137* (11), 3799-3802.

(20) Chang, S.-M.; Lin, C.-L.; Chen, Y.-J.; Wang, H.-C.; Chang, W.-C.; Lin, L.-Y., Improved Photovoltaic Performances of Dye-Sensitized Solar Cells with ZnO Films Co-Sensitized by Metal-Free Organic Sensitizer and N719 Dye. *Org. Electron.* **2015**, *25*, 254-260.

(21) Wu, Y.; Zhu, W.-H.; Zakeeruddin, S. M.; Grätzel, M., Insight into D–A−π–A Structured Sensitizers: A Promising Route to Highly Efficient and Stable Dye-Sensitized Solar Cells. *ACS Appl. Mater. Interfaces* **2015**, *7* (18), 9307-9318.

(22) Zhu, W.; Wu, Y.; Wang, S.; Li, W.; Li, X.; Chen, J.; Wang, Z. s.; Tian, H., Organic D ‐ A ‐ π ‐ A Solar Cell Sensitizers with Improved Stability and Spectral Response. *Adv. Funct. Mater.* **2011**, *21* (4), 756-763.

(23) Yen, Y. S.; Lee, C. T.; Hsu, C. Y.; Chou, H. H.; Chen, Y. C.; Lin, J. T., Benzotriazole ‐ Containing D–π–A Conjugated Organic Dyes for Dye ‐ Sensitized Solar Cells. *Chem. - Asian J.* **2013**, *8* (4), 809-816.

(24) Wu, Y.; Marszalek, M.; Zakeeruddin, S. M.; Zhang, Q.; Tian, H.; Grätzel, M.; Zhu, W., High-Conversion-Efficiency Organic Dye-Sensitized Solar Cells: Molecular Engineering on D–A–π-A Featured Organic Indoline Dyes. *Energy Environ. Sci.* **2012**, *5* (8), 8261-8272.

(25) Qu, S.; Wu, W.; Hua, J.; Kong, C.; Long, Y.; Tian, H., New Diketopyrrolopyrrole (DPP) Dyes for Efficient Dye-Sensitized Solar Cells. *J. Phys. Chem. C* **2009**, *114* (2), 1343-1349.

(26) Pei, K.; Wu, Y.; Li, H.; Geng, Z.; Tian, H.; Zhu, W. H., Cosensitization of D-A-π-A Quinoxaline Organic Dye: Efficiently Filling the Absorption Valley with High Photovoltaic Efficiency. *ACS Appl. Mater. Interfaces* **2015,** *7* (9), 5296-5304.

(27) Pei, K.; Wu, Y.; Islam, A.; Zhang, Q.; Han, L.; Tian, H.; Zhu, W., Constructing High-Efficiency D–A− π–A-featured Solar Cell Sensitizers: a Promising Building Block of 2, 3-Diphenylquinoxaline for Antiaggregation and Photostability. *ACS Appl. Mater. Interfaces* **2013**, *5* (11), 4986-4995.

(28) Xing, P.; Robertson, G. P.; Guiver, M. D.; Mikhailenko, S. D.; Wang, K.; Kaliaguine, S., Synthesis and Characterization of Sulfonated Poly (Ether Ether Ketone) for Proton Exchange Membranes. *J. Membr. Sci.* **2004**, *229* (1), 95-106.

(29) Duan, Y.; Tang, Q.; Chen, Y.; Zhao, Z.; Lv, Y.; Hou, M.; Yang, P.; He, B.; Yu, L., Solid-State Dye-Sensitized Solar Cells from Poly (Ethylene Oxide)/Polyaniline Electrolytes with

Catalytic and Hole-Transporting Characteristics. *J. Mater. Chem. A* **2015**, *3* (10), 5368-5374.

(30) Zheng, Z.; Chen, J.; Hu, Y.; Wu, W.; Hua, J.; Tian, H., Efficient Sinter-Free Nanostructure Pt Counter Electrode for Dye-Sensitized Solar Cells. *J. Mater. Chem. C* **2014**, *2* (40), 8497-8500.

(31) Wu, M.; Mu, L.; Wang, Y.; Lin, Y.-n.; Guo, H.; Ma, T., One-step Synthesis of Nano-Scaled Tungsten Oxides and Carbides for Dye-Sensitized Solar Cells as Counter Electrode Catalysts. *J. Mater. Chem. A* **2013**, *1* (25), 7519-7524.

(32) Wang, M.; Anghel, A. M.; Marsan, B. t.; Cevey Ha, N.-L.; Pootrakulchote, N.; Zakeeruddin, S. M.; Grätzel, M., CoS Supersedes Pt as Efficient Electrocatalyst for Triiodide Reduction in Dye-Sensitized Solar Cells. *J. Am. Chem. Soc.* **2009**, *131* (44), 15976-15977.

(33) Snaith, H. J.; Schmidt-Mende, L.; Grätzel, M.; Chiesa, M., Light Intensity, Temperature, and Thickness Dependence of the Open-Circuit Voltage in Solid-State Dye-Sensitized Solar Cells. *Phys. Rev. B* **2006**, *74* (4), 045306-1-6.

(34) Wu, Y.; Zhu, W., Organic Sensitizers from D–π–A to D–A–π–A: Effect of the Internal Electron-Withdrawing Units on Molecular Absorption, Energy Levels and Photovoltaic Performances. *Chem. Soc. Rev.* **2013**, *42* (5), 2039-2058.

(35) Kai, P.; Wu, Y.; Hui, L.; Geng, Z.; He, T.; Zhu, W. H., Cosensitization of D-A-π-A Quinoxaline Organic Dye: Efficiently Filling the Absorption Valley with High Photovoltaic Efficiency. *ACS Appl. Mater. Interfaces* **2015**, *7* (9), 5296-5304.

(36) Liu, B.; Zhu, W.; Zhang, Q.; Wu, W.; Xu, M.; Ning, Z.; Xie, Y.; Tian, H., Conveniently Synthesized Isophorone Dyes for High Efficiency Dye-Sensitized Solar Cells: Tuning

Photovoltaic Performance by Structural Modification of Donor Group in Donor–π–Acceptor System. *Chem. Commun.* **2009**, (13), 1766-1768.

(37) Ito, S.; Zakeeruddin, S. M.; Humphry‐Baker, R.; Liska, P.; Charvet, R.; Comte, P.; Nazeeruddin, M. K.; Péchy, P.; Takata, M.; Miura, H., High‐Efficiency Organic‐Dye‐Sensitized Solar Cells Controlled by Nanocrystalline‐TiO_2 Electrode Thickness. *Adv. Mater.* **2006**, *18* (9), 1202-1205.

(38) Xie, Y.; Wu, W.; Zhu, H.; Liu, J.; Zhang, W.; Tian, H.; Zhu, W.-H., Unprecedentedly Targeted Customization of Molecular Energy Levels with Auxiliary-Groups in Organic Solar Cell Sensitizers. *Chem. Sci.* **2016**, *7* (1), 544-549.

(39) Pei, K.; Wu, Y.; Wu, W.; Zhang, Q.; Chen, B.; Tian, H.; Zhu, W., Constructing Organic D–A–π‐A‐Featured Sensitizers with a Quinoxaline Unit for High‐Efficiency Solar Cells: The Effect of an Auxiliary Acceptor on the Absorption and the Energy Level Alignment. *Chem. - Eur. J.* **2012**, *18* (26), 8190-8200.

(40) Hu, Y.; Abate, A.; Cao, Y.; Ivaturi, A.; Zakeeruddin, S. M.; Grätzel, M.; Robertson, N., High Absorption Coefficient Cyclopentadithiophene Donor-Free Dyes for Liquid and Solid-State Dye-Sensitized Solar Cells. *J. Phys. Chem. C* **2016**, *120 (*28), 15027-15034.

(41) Bai, Y.; Zhang, J.; Zhou, D.; Wang, Y.; Zhang, M.; Wang, P., Engineering Organic Sensitizers for Iodine-Free Dye-Sensitized Solar Cells: Red-Shifted Current Response Concomitant with Attenuated Charge Recombination. *J. Am. Chem. Soc.* **2011**, *133* (30), 11442-11445.

(42) Frank, A. J.; Kopidakis, N.; Lagemaat, J. v. d., Electrons in Nanostructured TiO_2 Solar Cells: Transport, Recombination and Photovoltaic Properties. *Coord. Chem. Rev.* **2004,** *248* (13-14), 1165-1179.

(43) Cao, Y. M.; Bai Y.; Yu, Q. J.; Cheng, Y. M.; Liu, S.; Shi, D.; Gao, F. F.; and Wang, P., Dye-Sensitized Solar Cells with a High Absorptivity Ruthenium Sensitizer Featuring a 2-(Hexylthio)thiophene Conjugated Bipyridine. *J. Phys. Chem. C* **2009,** *113* (15), 6290-6297.

(44) Hagfeldt, A.; Boschloo, G.; Sun, L.; Kloo, L.; Pettersson, H., Dye-sensitized Solar Cells. *Chem. Rev.* **2010**, *110* (11), 6595-6663.

(45) Mathew, S.; Yella, A.; Gao, P.; Humphry-Baker, R.; Curchod, B. F.; Ashari-Astani, N.; Tavernelli, I.; Rothlisberger, U.; Nazeeruddin, M. K.; Grätzel, M., Dye-Sensitized Solar Cells with 13% Efficiency Achieved Through the Molecular Engineering of Porphyrin Sensitizers. *Nat. Chem.* **2014**, *6* (3), 242-247.

(46) Pandey, S. S.; Lee, K.-Y.; Hayat, A.; Ogomi, Y.; Hayase, S., Investigating the Role of Dye Dipole on Open Circuit Voltage in Solid-State Dye-Sensitized Solar Cells. *Jpn. J. Appl. Phys.* **2011**, *50* (6), 1271-1295.

(47) Tang, Q.; Yuan, S.; Cai, H., High-Temperature Proton Exchange Membranes from Microporous Polyacrylamide Caged Phosphoric Acid. *J. Mater. Chem. A* **2013**, *1* (3), 630-636.

(48) Wang, H.; Li, J.; Gong, F.; Zhou, G.; Wang, Z.-S., Ionic Conductor with High Conductivity as Single-Component Electrolyte for Efficient Solid-State Dye-Sensitized Solar Cells. *J. Am. Chem. Soc.* **2013**, *135* (34), 12627-12633.

(49) Hanwell, M. D.; Curtis, D. E.; Lonie, D. C.; Vandermeersch, T.; Zurek, E.; Hutchison, G. R., Avogadro: an Advanced Semantic Chemical Editor, Visualization, and Analysis Platform. *J. Cheminf.* **2012**, *4* (1), 1-17.

(50) Bauernschmitt, R.; Ahlrichs, R., Treatment of Electronic Excitations within the Adiabatic Approximation of Time Dependent Density Functional Theory. *Chem. Phys. Lett.* **1996**, *256* (4), 454-464.

(51) Tozer, D. J.; Handy, N. C., Improving Virtual Kohn–Sham Orbitals and Eigenvalues: Application to Excitation Energies and Static Polarizabilities. *J. Chem. Phys.* **1998**, *109* (23), 10180-10189.

(52) Yanai, T.; Tew, D. P.; Handy, N. C., A New Hybrid Exchange–Correlation Functional Using the Coulomb-Attenuating Method (CAM-B3LYP). *Chem. Phys. Lett.* **2004**, *393* (1), 51-57.

(53) O'boyle, N. M.; Tenderholt, A. L.; Langner, K. M., Cclib: a Library for Package‐Independent Computational Chemistry Algorithms. *J. Comput. Chem.* **2008**, *29* (5), 839-845.

D-A-π-A Motif Quinoxaline-Based Sensitizers with High Molar Extinction Coefficient for Quasi-Solid State Dye-sensitized Solar Cells

Yu Wang, Zhiwei Zheng, Tianyue Li, Neil Robertson, Huaide Xiang, Wenjun Wu*, Jianli Hua, Wei-Hong Zhu, and He Tian

A novel D-A-π-A configuration organic sensitizer **IQ22** was specifically designed with broad light response and high molar extinction coefficient for increasing the short-circuit current density (J_{SC}), and improving the open-circuit voltage (V_{OC}). And a promising conversion efficiency as high as 8.76% was got, standing out in the Qs-DSSCs utilizing metal-free organic sensitizers.